Purcell effect in wire metamaterials

Alexander N. Poddubny,[1,2,*] Pavel A. Belov,[1] and Yuri S. Kivshar[1,3]

[1]*National Research University for Information Technology, Mechanics and Optics, St. Petersburg 197101, Russia*

[2]*Ioffe Physical-Technical Institute of the Russian Academy of Sciences, St. Petersburg 194021, Russia*

[3]*Nonlinear Physics Center and Center for Ultrahigh-Bandwidth Devices for Optical Systems, Research School of Physics and Engineering, Australian National University, Canberra ACT 0200, Australian Capital Territory, Australia*

(Received 2 September 2012; revised manuscript received 13 January 2013; published 28 January 2013)

We study theoretically the enhancement of spontaneous emission in wire metamaterials. We analyze the dependence of the Purcell factor on the wire dielectric constant for both electric and magnetic dipole sources and find an optimal value of the dielectric constant for maximizing the Purcell factor for the electric dipole. We obtain analytical expressions for the Purcell factor and also provide estimates for the Purcell factor in realistic structures operating in both microwave and optical spectral ranges.

DOI: 10.1103/PhysRevB.87.035136 PACS number(s): 41.20.Jb, 42.50.−p, 81.05.Xj, 78.67.Ch

I. INTRODUCTION

Wire metamaterials are composed of arrays of optically thin metallic rods embedded in a dielectric matrix (see Ref. 1 and references therein). Experimental realizations of such structures span from microwaves[2] to optics,[3–7] and they are very promising for a number of applications, including the subwavelength transmission of images,[2] negative refraction phenomena,[8] superlensing,[9] and biosensing applications.[5] Strong enhancement of the Vavilov-Cherenkov radiation and peculiar dipole emission patterns has been also predicted for wire metamaterials.[10–12]

A specific property of wire metamaterials is the strong nonlocality of the effective dielectric response,[13] manifested as the formation of so-called TEM modes in addition to the TE and TM modes of an ordinary uniaxial structure. Due to a finite value of the dielectric constant of wires, TEM modes acquire hyperbolic dispersion.[14] In this regard the wire medium represents a particular class of metamaterials with hyperbolic isofrequency surfaces, which have recently attracted a lot of attention.[15,16] A specific feature of the hyperbolic metamaterials is a diverging photonic density of states, promoting a high spontaneous decay rate of the embedded light source.[17,18] In wire metamaterials this effect should lead to a large Purcell factor as well.

In realistic structures the divergence in the photonic density of states and Purcell factor is canceled due to the cutoff arising for large wave vectors. Reasons for the cutoff include (i) finite size of the emitter,[17,19,20] (ii) spatial dispersion,[21] and (iii) finite size of the metamaterial unit cell.[22–25] Case iii is realized when the emitter, e.g., a semiconductor quantum dot, is smaller than the unit-cell size, so that the Purcell factor is strongly sensitive to the structure geometry. Consequently, the detailed theory recently developed for planar metal-dielectric metamaterials[18,22,23] is not applicable directly to nanowire arrays, and a novel study is required. The crude estimation of the Purcell factor[26] is provided by the density-of-states enhancement of TEM modes $\sim(\lambda/a)^2$, where λ is the wavelength and a is the structure period. In this paper we aim to perform more comprehensive analysis which takes into account a finite dielectric constant of the wires and allows for arbitrary spatial position of the source in the metamaterial unit cell. We consider both *electric* and *magnetic* dipole sources, because high sensitivity of the enhancement factor to the dipole source type has been known since the original work of Purcell.[27,28]

The paper is organized as follows. Section II presents our theoretical model. Section III is devoted to the analysis of the eigenmode dispersion of the structure. Section IV contains numerical and analytical results for the Purcell factor. Discussion of the Purcell factor attainable in different experimental conditions is summarized in Sec. V, and the last section concludes the paper.

II. LOCAL-FIELD APPROACH

The structure under consideration is illustrated schematically in Fig. 1. It consists of identical infinitely long wires with radius R, arranged in an infinite square lattice with the period a and parallel to z axis. Wires are characterized with the dielectric constant $\varepsilon_{\text{wire}}$ and embedded in a vacuum. The electric or magnetic dipole source is positioned in the structure at the point $\boldsymbol{r}_0 \equiv \boldsymbol{\rho}_0 + z_0\hat{\boldsymbol{z}}$. The electric field satisfies the following equation:

$$\nabla \times \nabla \times \boldsymbol{E} - q^2\varepsilon(\boldsymbol{\rho})\boldsymbol{E} = 4\pi q^2 \boldsymbol{P}, \tag{1}$$

where

$$\varepsilon(\boldsymbol{\rho}) = 1 + (\varepsilon_{\text{wire}} - 1)\sum_{\boldsymbol{\rho}_j}\theta(R - |\boldsymbol{\rho} - \boldsymbol{\rho}_j|) \tag{2}$$

is the dielectric function (here θ is the Heaviside step function);

$$\boldsymbol{P} = \begin{cases} \boldsymbol{p}\,\delta(\boldsymbol{r} - \boldsymbol{r}_0) & \text{(electric dipole)} \\ \frac{\mathrm{i}}{q}\nabla \times \boldsymbol{m}\delta(\boldsymbol{r} - \boldsymbol{r}_0) & \text{(magnetic dipole)} \end{cases} \tag{3}$$

is the polarization term, describing the electric or magnetic point-dipole source with electric or magnetic momentum $\boldsymbol{p}$ or $\boldsymbol{m}$, respectively; and $q = \omega/c$. Scaling of the dielectric function Eq. (2) allows us to generalize the model for the arbitrary real dielectric constant of the matrix. The vectors $\boldsymbol{\rho}_j$ in Eq. (2) belong to the two-dimensional square lattice. We neglect the transverse polarizability of the wires, assuming that they are much thinner than the light wavelength $\lambda = 2\pi/q$. Therefore, wire polarization per unit length is solely described

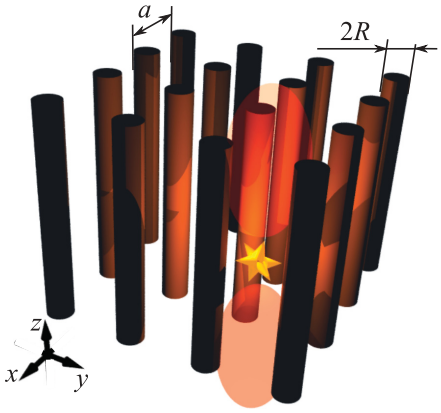

FIG. 1. (Color online) Scheme of a wire metamaterial with an embedded light source.

by nonlocal axial polarizability α, determined from

$$\boldsymbol{P}(z) = \int \frac{\mathrm{d}k_z}{2\pi} \mathrm{e}^{\mathrm{i}k_z z} \alpha(k_z) \hat{\boldsymbol{z}} E_z(k_z) \tag{4}$$

and given by[13,14,29]

$$\frac{1}{\alpha} \approx -\mathrm{i}\pi q_\perp^2 H_0^{(1)}(q_\perp R) + \frac{4}{(\varepsilon_{\text{wire}} - 1)R^2}, \tag{5}$$

where $q_\perp^2 = q^2 - k_z^2$, and $H_0^{(1)}$ is the zeroth-order Hankel function of the first kind. The essential feature of Eq. (5) is the spatial dispersion of the wire dielectric response, i.e., the dependence of the polarizability on the wave vector k_z.

The Purcell factor for electric $[f^{(e)}]$ and magnetic $[f^{(m)}]$ dipole emission may be found via the imaginary part of electric field $\boldsymbol{E}$ and magnetic field $\boldsymbol{H}$, induced in the structure by the source:[28,30,31]

$$\begin{aligned} f^{(e)} &= \frac{3}{2q^3 p^2} \operatorname{Im}[\boldsymbol{E}(\boldsymbol{r}_0) \cdot \boldsymbol{p}], \\ f^{(m)} &= \frac{3}{2q^3 m^2} \operatorname{Im}[\boldsymbol{H}(\boldsymbol{r}_0) \cdot \boldsymbol{m}]. \end{aligned} \tag{6}$$

The field is given by a sum over Bloch waves with wave vectors $\boldsymbol{k} = \boldsymbol{k}_\perp + k_z \hat{\boldsymbol{z}}$, similar to the case of a cubic dipole lattice.[24] The Purcell factors $f^{(e,m)}$ for both electric and magnetic emission can be presented in the following general form:

$$\begin{aligned} f^{(e,m)} = 1 + \frac{3a^2}{2q^3} \operatorname{Im} \int_{-\infty}^{\infty} \frac{\mathrm{d}k_z}{2\pi} \int_{-\pi/a}^{\pi/a} \frac{\mathrm{d}k_x}{2\pi} \int_{-\pi/a}^{\pi/a} \\ \times \frac{\mathrm{d}k_y}{2\pi} \frac{[\boldsymbol{G}_{\boldsymbol{k}}^{(e,m)}(\boldsymbol{\rho}_0) \cdot \boldsymbol{n}][\boldsymbol{G}_{\boldsymbol{k}}^{(e,m)}(-\boldsymbol{\rho}_0) \cdot \boldsymbol{n}]}{1/\alpha(\boldsymbol{k}) - C(\boldsymbol{k}) - \mathrm{i}\delta}. \end{aligned} \tag{7}$$

Here, $\boldsymbol{n}$ is the unit vector oriented along the dipole. The quantity $-\mathrm{i}\delta$ in the denominator of Eq. (7) is the infinitesimal imaginary term; the limit $\delta \to 0$ should be taken after the integral over $\boldsymbol{k}$ is calculated. The quantity C in Eq. (7) is the interaction constant of the wires,[29] defined as

$$C(\boldsymbol{k}) = \mathrm{i}\pi q_\perp^2 \sum_{\boldsymbol{\rho}_j \neq 0} \mathrm{e}^{\mathrm{i}\boldsymbol{k}_\perp \boldsymbol{\rho}_j} H_0^{(1)}(q\rho_j), \tag{8}$$

and

$$\boldsymbol{G}_{\boldsymbol{k}}^{(e,m)}(\boldsymbol{\rho}) = \sum_{\boldsymbol{\rho}_j} \boldsymbol{G}_0^{(e,m)}(\boldsymbol{\rho} - \boldsymbol{\rho}_j, k_z) \mathrm{e}^{\mathrm{i}\boldsymbol{k} \cdot (\boldsymbol{\rho} - \boldsymbol{\rho}_j)} \tag{9}$$

is the periodic Green's function for waves with Bloch vector $\boldsymbol{k}_\perp$. Here, $\boldsymbol{G}_0^{(e)}$ and $\boldsymbol{G}_0^{(m)}$ are electric and magnetic fields, respectively, of a single polarized wire, given by

$$\boldsymbol{G}_0^{(e)}(\boldsymbol{\rho}, k_z) = \mathrm{i}\pi q_\perp^2 \hat{\boldsymbol{z}} H_0^{(1)}(q_\perp \rho) + \pi k_z q_\perp \hat{\boldsymbol{\rho}} H_1^{(1)}(q_\perp \rho), \tag{10}$$

for the electric dipole, and

$$\boldsymbol{G}_0^{(m)}(\boldsymbol{\rho}, k_z) = \pi q_\perp q \hat{\boldsymbol{\varphi}} H_1^{(1)}(q_\perp \rho), \tag{11}$$

for the magnetic dipole. Equations (7)–(11) present results for the Purcell factor. In practical calculations, however, the series Eqs. (8) and (9) should be evaluated not directly but using either the Ewald summation[32] or a Floquet-type summation.[29] The latter approach turns out to be more numerically efficient; it yields the following result:[13,29]

$$\begin{aligned} C(\boldsymbol{k}) = -2q_\perp^2 \ln \frac{2\pi R}{a} - \sum_{m=-\infty}^{\infty} \left(\frac{2\pi q_\perp^2}{q_{x,m} a} \frac{\sin q_{x,m} a}{\cos q_{x,m} a - \cos k_x a} \right. \\ \left. - \frac{q_\perp^2 (1 - \delta_{m,0})}{|m|} \right), \end{aligned} \tag{12}$$

for the interaction constant, where $q_{x,m} = \sqrt{q^2 - k_z^2 - k_{y,m}^2}$ and $k_{y,m} = k_y + 2\pi m/a$. A similar technique can be used to calculate the Green's function; the corresponding result reads

$$\boldsymbol{G}_{\boldsymbol{k}}^{(e)}(\boldsymbol{\rho}) = \sum_{m=-\infty}^{\infty} (-q_\perp^2 \mathcal{S}_m \hat{\boldsymbol{z}} - \mathrm{i}k_z q_{x,m} \mathcal{C}_m \hat{\boldsymbol{x}} + k_{y,m} k_z \mathcal{S}_m \hat{\boldsymbol{y}}), \tag{13}$$

where

$$\begin{aligned} \mathcal{S}_m &= \frac{2\pi}{q_{x,m} a} \frac{\mathrm{e}^{\mathrm{i}k_x a} \sin q_{x,m} x - \sin q_{x,m}(x - a)}{\cos k_x a - \cos q_{x,m} a} \mathrm{e}^{\mathrm{i}k_{y,m} y}, \\ \mathcal{C}_m &= \frac{2\pi}{q_{x,m} a} \frac{\mathrm{e}^{\mathrm{i}k_x a} \cos q_{x,m} x - \cos q_{x,m}(x - a)}{\cos k_x a - \cos q_{x,m} a} \mathrm{e}^{\mathrm{i}k_{y,m} y}. \end{aligned} \tag{14}$$

The Green's function $\boldsymbol{G}_{\boldsymbol{k}}^{(m)}$ can be obtained from Eqs. (13) and (14) using the following expression:

$$\boldsymbol{G}_{\boldsymbol{k}}^{(m)} = \frac{1}{q} (\hat{\boldsymbol{x}} \partial_x + \hat{\boldsymbol{y}} \partial_y + \mathrm{i}k_z \hat{\boldsymbol{z}}) \times \boldsymbol{G}_{\boldsymbol{k}}^{(e)}. \tag{15}$$

Below we present numerical results for the Purcell factor along with analytical answers in certain limiting cases. We first determine analytical expressions for the dispersion of the eigenmodes of the structure (Sec. III) and then analyze the dependence of the Purcell factor on the dielectric constant of the wires (Sec. IV A) and on the source position (Sec. IV B).

III. DISPERSION ANALYSIS

The spontaneous decay is due to the emission of photons, with dispersion found from the zeros of the resonant denominator in Eq. (7):

$$\frac{1}{\alpha(\boldsymbol{k})} - C(\boldsymbol{k}) = 0. \tag{16}$$

Using Eqs. (5) and (12) we can present Eq. (16) for $qa \ll 1$ and $ka \ll 1$ as

$$\frac{1}{\alpha} - C \approx -\frac{4\pi}{a^2 q_p^2}\left[\left(q^2 - k_z^2\right)\left(\frac{q_p^2}{k^2 - q^2} + 1\right) + \varkappa^2\right], \quad (17)$$

where

$$\varkappa^2 = q_p^2 \frac{a^2}{\pi(1-\varepsilon_{\rm wire})R^2}, \quad \frac{1}{q_p^2} \approx \frac{a^2}{2\pi}\left[\ln\left(\frac{a}{2\pi R}\right) + \frac{\pi}{6}\right]. \quad (18)$$

Here, the wave vector $\varkappa \propto 1/\sqrt{1-\varepsilon_{\rm wire}}$ characterizes the finite value of the wire dielectric constant and q_p is the effective plasma wave vector. Equation (17) can be rewritten as

$$\frac{1}{\alpha} - C \approx -\frac{4\pi}{a^2 q_p^2}\frac{\left(k_z^2 - k_1^2\right)\left(k_z^2 - k_2^2\right)}{k_{\rm TM}^2 + q_p^2 - k_z^2}, \quad (19)$$

where

$$k_{1,2}^2 = \frac{q^2 + \varkappa^2 + k_{\rm TM}^2}{2} \pm \sqrt{\frac{1}{4}\left(q^2 + \varkappa^2 - k_{\rm TM}^2\right)^2 - q_p^2\varkappa^2} \quad (20)$$

are the z components of the wave vectors of the eigenmodes of the wire medium and

$$k_{\rm TM} = \sqrt{q^2 - k_\perp^2 - q_p^2}. \quad (21)$$

Eigenmodes Eq. (20) can be also obtained if the wire medium is treated as a homogeneous medium with spatial dispersion,[14] where the nonlocal effective dielectric constant reads

$$\varepsilon_{xx} = \varepsilon_{yy} = 1, \quad \varepsilon_{zz} = 1 - \frac{q_p^2}{q^2 - \varkappa^2 - k_z^2}. \quad (22)$$

For large values of the wire dielectric constant ($\varepsilon_{\rm wire} \gg 1$), when $\varkappa$ is small, Eqs. (20) may be approximately rewritten as

$$k_1^2 \approx q^2 + \frac{\varkappa^2 k_\perp^2}{q_p^2 + k_\perp^2}, \quad k_2^2 \approx q^2 - q_p^2 - k_\perp^2 + \frac{\varkappa^2 q_p^2}{q_p^2 + k_\perp^2}. \quad (23)$$

For perfect wires with $\varepsilon_{\rm wire} \to \infty$ Eqs. (23) reduce to

$$\begin{aligned} k_1 &= q(\text{TEM mode}), \\ k_2 &= k_{\rm TM}(\text{TM mode}). \end{aligned} \quad (24)$$

The dispersionless TEM modes are specific for the wire medium.[13] Both electric and magnetic fields for these modes are transverse to the wire axes. For $q < q_p$ TEM modes are the only propagating modes in the structure and solely control the spontaneous emission rate. Due to the high density of TEM photonic states one can expect a large Purcell factor.[26] For finite values of $\varepsilon_{\rm wire}$, TEM and TM modes mix, as can be seen from Eqs. (20).

Figure 2 presents isofrequency curves of quasi-TEM modes $k_1^{(z)}$ for different values of the wire dielectric constant. Thick black curves are obtained from numerical solution of Eq. (16), with α and C found from Eqs. (5) and (12), respectively. Thin red curves present approximate analytical answer Eq. (23). Thick solid and thick dashed curves correspond to the cases of

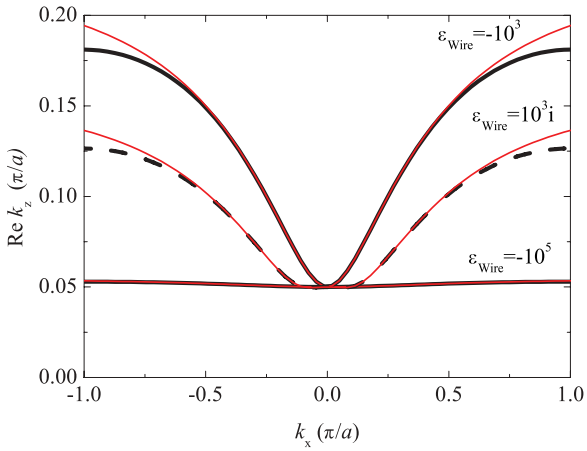

FIG. 2. (Color online) Isofrequency curves for quasi-TEM modes calculated for the different values of the wire dielectric constant $\varepsilon_{\rm wire}$. Thick curves are numerical solutions of Eq. (16), and thin curves are plotted according to approximate Eq. (23). Calculation was performed at $qa = 0.05\pi$ and $R/a = 0.05$.

"superconducting" and "conducting" wires, $\varepsilon_{\rm wire} = -|\varepsilon_{\rm wire}|$ (the permittivity is entirely real and negative) and $\varepsilon_{\rm wire} = {\rm i}|\varepsilon_{\rm wire}|$ (the permittivity is entirely imaginary and positive), respectively. Figure 2 shows that for finite values of $\varepsilon_{\rm wire}$ the TEM modes acquire *hyperboliclike dispersion*, and the absolute values of the wave vector k_z increase according to Eq. (23). The growth of the wave vector k_z for nonperfectly conducting wires is illustrated in Fig. 3(a). Another effect of the finite dielectric constant is the decrease of the effective plasma wave vector, defined as the cutoff of TM waves:

$$\tilde{q}_p^2 \equiv q^2 - k_2^2(k_\perp = 0) \approx q_p^2 - \varkappa^2. \quad (25)$$

Equation (25) indicates that the plasma frequency $c\tilde{q}_p$ becomes smaller for nonperfect wires. Corresponding dependence is shown in Fig. 3(b). For small enough values of $\varepsilon_{\rm wire} \sim -(1/\pi)(a/R)^2$, the plasma frequency vanishes. This means that the wire medium can be no longer considered as a single-mode hyperbolic metamaterial, because TM modes become propagating in addition to the TEM modes.

IV. PURCELL FACTOR

Now we proceed to the analysis of the dependence of the Purcell factor on the wire dielectric constant (Sec. IV A) and on the dipole position within the unit cell of the structure (Sec. IV B).

A. Effect of wire dielectric constant

In this section we focus on the case of the source located in the center of the unit cell, $x_0 = y_0 = a/2$, and analyze the dependence of the Purcell factor on the dielectric constant of the wires $\varepsilon_{\rm wire}$. We first obtain analytical results for the Purcell factor and then compare them with direct numerical integration of Eq. (7).

In order to integrate Eq. (7) analytically, it is useful to rewrite the Green's function Eq. (9) in the following equivalent

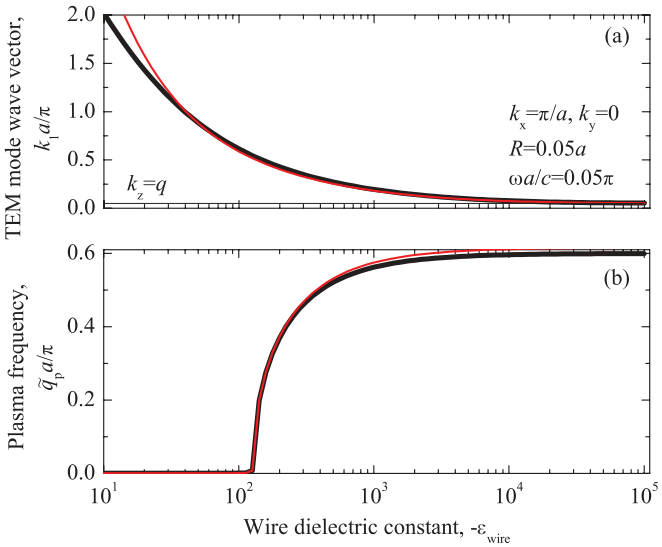

FIG. 3. (Color online) Quasi-TEM mode (a) wave vector and (b) effective plasma frequency $\tilde{q}_p$ as functions of the wire dielectric constant. Thick black and thin red lines correspond to the numerical solution of Eq. (16) and analytical Eqs. (23), respectively. Calculation was performed for $\varepsilon_{\text{wire}} = -|\varepsilon_{\text{wire}}|$, $qa = 0.05\pi$, $R/a = 0.05$, and $x_0 = y_0 = a/2$.

form:

$$\boldsymbol{G}_{\boldsymbol{k}}^{(e)}(\boldsymbol{\rho}) = -\frac{4\pi}{a^2}\sum_{\boldsymbol{b}}\frac{(q^2-k_z^2)\hat{\boldsymbol{z}}-k_z(\boldsymbol{k}_\perp+\boldsymbol{b})}{q^2-k_z^2-(\boldsymbol{k}_\perp+\boldsymbol{b})^2}\mathrm{e}^{\mathrm{i}(\boldsymbol{k}_\perp+\boldsymbol{b})\boldsymbol{\rho}}, \tag{26}$$

$$\boldsymbol{G}_{\boldsymbol{k}}^{(m)}(\boldsymbol{\rho}) = -\frac{4\pi q}{a^2}\sum_{\boldsymbol{b}}\frac{\hat{\boldsymbol{z}}\times(\boldsymbol{k}_\perp+\boldsymbol{b})}{q^2-k_z^2-(\boldsymbol{k}_\perp+\boldsymbol{b})^2}\mathrm{e}^{\mathrm{i}(\boldsymbol{k}_\perp+\boldsymbol{b})\boldsymbol{\rho}}. \tag{27}$$

Here $\boldsymbol{b}$ are the reciprocal vectors of the square lattice. Equations (26) and (27) can be obtained by applying the Poisson summation formula to Eq. (9).[33] Terms with $\boldsymbol{b} \neq 0$ in Eqs. (26) and (27) correspond to the short-range component of the field of the wires and strongly depend on $\boldsymbol{\rho}$. In the case where the dipole is located in the unit-cell center, $x_0 = y_0 = a/2$, the contribution of the short-range component is minimized and the Green's function can be satisfactorily described by the long-range component only, given by the term with $b = 0$. A relatively simple analytical expression for the Purcell factor can be obtained if only the residue at the wave vector of the quasi-TEM mode with $k_z \equiv k_{1,z}$ is taken into account in Eq. (7). This means that the integration over k_z is performed according to the following rule:

$$\lim_{\delta\to 0}\int\frac{dk_z}{2\pi}\frac{F(k_z)}{(1/\alpha)-C-\mathrm{i}\delta} = \mathrm{i}\frac{a^2q_p^2}{4\pi}F(k_{1,z})\frac{k_{\mathrm{TM}}^2+q_p^2-k_1^2}{2k_1\left(k_2^2-k_1^2\right)}, \tag{28}$$

where $F(k_z)$ is an arbitrary or even analytical function of k_z. Equation (28) is obtained using the approximate Eq. (19) for the denominator $1/\alpha - C$. Substituting the terms with $b = 0$ from Eqs. (26) and (27) into Eq. (7) and integrating over k_z following Eq. (28) we reduce the Purcell factor to the integrals over in-plane wave vector $k_\perp$:

$$f_x^{(e)} = f_y^{(e)} = \frac{3q_p^2}{4q^2}\,\mathrm{Re}\int_0^{K_{\max}}\frac{\mathrm{d}k_\perp k_\perp\left(q_p^2+\nu k_\perp^2\right)^{1/2}}{\left(q_p^2+k_\perp^2\right)^{3/2}},$$

$$f_z^{(e)} = \frac{3\varkappa^4}{4q^4}\,\mathrm{Re}\int_0^{K_{\max}}\frac{\mathrm{d}k_\perp k_\perp^3 q_p^2}{\left(q_p^2+k_\perp^2\right)^{5/2}\left(q_p^2+\nu k_\perp^2\right)^{1/2}},$$

$$f_x^{(m)} = f_y^{(m)} = \frac{3q_p^2}{4q^2}\,\mathrm{Re}\int_0^{K_{\max}}\frac{\mathrm{d}k_\perp k_\perp}{\left(q_p^2+k_\perp^2\right)^{1/2}\left(q_p^2+\nu k_\perp^2\right)^{1/2}},$$

$$f_z^{(m)} = 1. \tag{29}$$

Here, the coefficient

$$\nu = 1+\frac{\varkappa^2}{q^2} \equiv 1+\frac{q_p^2}{q^2}\frac{a^2}{\pi(1-\varepsilon_{\text{wire}})R^2} \tag{30}$$

accounts for a finite dielectric constant of the wires. The integrands in Eqs. (29) are smooth functions of the transverse wave vector. Consequently, in order to simplify the analysis, we replace the integration over the quadratic Brillouin zone in Eqs. (29) by integration over the effective circular Brillouin zone. Within this approximation the circular Brillouin-zone radius $K_{\max}$ is a phenomenological cutoff parameter; its value has been chosen equal to $2\sqrt{\pi}/a$ to ensure that the size of the Brillouin zone in circular approximation remains the same, $\pi K_{\max}^2 = (2\pi/a)^2$. It will be shown below that this crude approximation well describes the result of direct numerical integration of Eq. (7). After the integration in Eqs. (29), we obtain

$$f_{x,y}^{(e)} = \frac{3q_p^2}{8q^2}\,\mathrm{Re}\left[-\frac{2\beta}{\alpha}+2+2\sqrt{\nu}\ln\frac{\alpha\sqrt{\nu}+\beta}{\sqrt{\nu}+1}\right], \tag{31}$$

$$f_z^{(e)} = \mathrm{Re}\,\frac{\beta(\beta^2-3\alpha^2)}{4\alpha^3}+\frac{1}{2}, \tag{32}$$

$$f_{x,y}^{(m)} = \frac{3q_p^2}{8q^2}\,\mathrm{Re}\,\frac{2}{\sqrt{\nu}}[\ln(\sqrt{\nu}\alpha+\beta)-\ln(\sqrt{\nu}+1)]. \tag{33}$$

In the limit of perfectly conducting wires ($|\varepsilon_{\text{wire}}| \to \infty$) Eqs. (31)–(33) reduce to

$$f_{x,y}^{(e)} = f_{x,y}^{(m)} = \tfrac{3}{8}\tfrac{q_p^2}{q^2}\ln\left(1+\tfrac{K_{\max}^2}{q_p^2}\right), \tag{34}$$

$$f_z^{(e)} = 0, \tag{35}$$

$$f_z^{(m)} = 1. \tag{36}$$

Since $q_p \sim 1/a$, the Purcell factor can be estimated by the order of magnitude as $(\lambda/a)^2$ where $\lambda = 2\pi/q$.

Calculated dependence of the electric and magnetic Purcell factors on the wire dielectric constant is presented in Fig. 4. For an infinite value of the wire dielectric constant $\varepsilon_{\text{wire}}$ the Purcell factor is enhanced only for in-plane dipoles which can couple to the TEM waves. It is equal for the electric and magnetic dipoles, according to Eq. (34). The figure demonstrates that the Purcell factor for the in-plane electric dipole grows for the finite dielectric constant (black curves). Moreover, spontaneous emission for the vertical electric dipole becomes possible, and its rate strongly increases for smaller values of $\varepsilon_{\text{wire}}$. In the limit $\varepsilon_{\text{wire}} \to \infty$ the Purcell factor does not depend on the phase of the wire dielectric constant. For

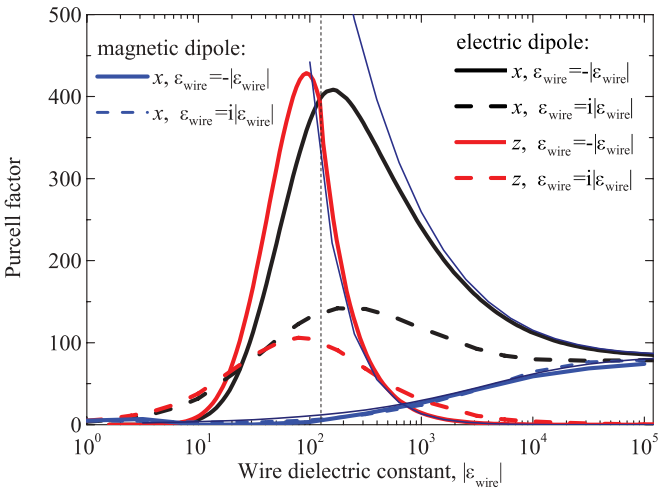

FIG. 4. (Color online) Purcell factor for electric and magnetic dipoles as function of the wire dielectric constant. Thick black, red, and blue lines correspond to in-plane electric, vertical electric, and in-plane magnetic dipole, respectively. Solid and dashed lines are calculated for $\varepsilon_{\text{wire}}$ changing along imaginary and real axes, $\varepsilon_{\text{wire}} = \mathrm{i}\varepsilon_{\text{wire}}$ and $-|\varepsilon_{\text{wire}}|$, respectively. Thick lines are calculated by direct numerical integration of Eq. (7), and thin lines present approximate analytical results Eqs. (31)–(33). The thin vertical dotted line indicates the cutoff value of the wire dielectric constant, corresponding to the condition $\tilde{q}_p(\varepsilon_{\text{wire}}) = 0$. Calculation was performed at $qa = 0.05\pi$, $R/a = 0.05$, and $x_0 = y_0 = a/2$.

the finite dielectric constant the value of the Purcell factor depends on the phase and grows both for "superconducting" wires ($\mathrm{Re}\,\varepsilon_{\text{wire}} < 0$, $\mathrm{Im}\,\varepsilon_{\text{wire}} = 0$, solid curves in Fig. 4) and for "conducting" wires ($\mathrm{Re}\,\varepsilon_{\text{wire}} = 0$, $\mathrm{Im}\,\varepsilon_{\text{wire}} > 0$, dashed curves in Fig. 4). For relatively large values of $|\varepsilon_{\text{wire}}|$ the results of direct numerical integration of Eq. (7) (thick curves) are well described by analytical Eqs. (31) and (32) (thin curves).

The origin of the Purcell factor enhancement for finite values of $\varepsilon_{\text{wire}}$ can be explained by a competition of two effects: (i) dependence of the wire electric field $\boldsymbol{G}_{\boldsymbol{k}}^{(e)}$ on the quasi-TEM mode wave vector k_z and (ii) density-of-states dependence on k_z. As demonstrated by Figs. 2 and 3(a), the values of k_z for quasi-TEM modes grow for smaller $\varepsilon_{\text{wire}}$. Equation (10) shows that both in-plane and axial components of the Green's function increase with k_z due to the prefactor before Hankel functions. For a given value of $k_\perp$ the density of states effectively decreases with k_z, which is described by the $1/k_1$ factor in Eq. (28). Since the Purcell factor Eq. (7) is proportional to the square of the Green's function times the density of states, it still grows for smaller values of $\varepsilon_{\text{wire}}$. The optimum value of the Purcell factor is reached for the dielectric constant $|\varepsilon_{\text{wire}}| \sim (1/\pi)(a/R)^2$. This approximately corresponds to the condition of vanishing effective plasma frequency $\tilde{q}_p(\varepsilon_{\text{wire}})$ (see the vertical dotted line in Fig. 4). The situation is different for the magnetic dipole. In contrast to the electric dipole case, the in-plane components of the corresponding Green's function Eq. (11) lack the prefactor k_z. Consequently, the Purcell factor for the in-plane magnetic dipole is quenched for smaller values of the wire dielectric constant, in agreement with Fig. 3 (blue curves).

The growth of the Purcell factor for smaller values of $\varepsilon_{\text{wire}}$ is in qualitative agreement with the local effective-medium model of a hyperbolic medium with an embedded finite-size source[17] and with the model of a layered metal dielectric hyperbolic metamaterial.[23] It has been demonstrated in Refs. 17 and 23 that the maximum value of the Purcell factor is reached when one of the components of the local dielectric tensor approaches zero from the negative side. The quantitatively correct effective-medium model of the wire metamaterial should be based on the nonlocal dielectric constant Eq. (22). Equations (31)–(33) are equivalent to the results of such a nonlocal effective model with the artificial wave-vector cutoff at $k = K_{\max}$.

B. Effect of dipole position

Hereafter we focus on perfect wires with $|\varepsilon_{\text{wire}}| \to \infty$ and analyze how the Purcell factor depends on the coordinate $\boldsymbol{\rho}_0 = (x_0, y_0)$ of the light source. For a dipole close enough to the wires, the Bloch Green's function Eq. (9) is mainly determined by the field of the nearest wire:

$$\boldsymbol{G}_{\boldsymbol{k}}(\boldsymbol{\rho}) \approx \boldsymbol{G}_0(\boldsymbol{\rho}). \tag{37}$$

For electric and magnetic dipoles, this leads to

$$\begin{aligned} \boldsymbol{G}^{(e)}(k_z = q) &\approx -2\mathrm{i}\frac{q\hat{\boldsymbol{\rho}}}{\rho}\mathrm{e}^{\mathrm{i}qz}, \\ \boldsymbol{G}^{(e)}(k_z = q) &\approx -2\mathrm{i}\frac{q\hat{\boldsymbol{\varphi}}}{\rho}\mathrm{e}^{\mathrm{i}qz}. \end{aligned} \tag{38}$$

Equation (38) indicates that for perfect wires only in-plane electric and magnetic dipoles couple with TEM waves. Thus, only for this orientation the Purcell factor is enhanced due to the large density of TEM waves. For perfect wires, the rule Eq. (28) for integration over k_z reduces to

$$\int \frac{\mathrm{d}k_z}{2\pi}\frac{F(k_z)}{1/\alpha - C - \mathrm{i}\delta} = \frac{\mathrm{i}F(q)}{2q}\frac{a^2}{4\pi}\frac{1}{\dfrac{1}{k_\perp^2} + \dfrac{1}{q_p^2}}. \tag{39}$$

The integral is totally determined by the residue at the wave vector corresponding to the TEM modes. Substituting Eqs. (38) and (39) into Eq. (7) we obtain

$$f^{(e)} = \frac{3a^4 q_p^2}{8\pi^2 q^2}\frac{(\hat{\boldsymbol{\rho}}_0 \cdot \boldsymbol{n})^2}{\rho_0^2}\int_0^{K_{\max}} \frac{k_\perp^3 \mathrm{d}k_\perp}{k_\perp^2 + q_p^2}. \tag{40}$$

Here, we have used the circular approximation of the square Brillouin zone, similarly to Eqs. (29). After the integration in Eq. (40) we obtain

$$\begin{aligned} f^{(e)} = \frac{(\hat{\boldsymbol{\rho}}_0 \cdot \boldsymbol{n})^2 a^2}{\rho_0^2}\frac{3}{16\pi^2 q^2 a^2} \\ \times\left[K_{\max}^2 q_p^2 a^4 - q_p^4 a^4 \ln\left(1 + \frac{K_{\max}^2}{q_p^2}\right)\right]. \end{aligned} \tag{41}$$

For the magnetic dipole one has

$$f^{(m)}(\boldsymbol{n}) = f^{(e)}(\boldsymbol{n} \times \hat{\boldsymbol{z}}); \tag{42}$$

i.e., the Purcell factor for the electric dipole, parallel to the radius vector $\boldsymbol{\rho}_0 \equiv x_0\hat{\boldsymbol{x}} + y_0\hat{\boldsymbol{y}}$, is the same as for the in-plane magnetic dipole, perpendicular to $\boldsymbol{\rho}_0$. Equation (42) is the

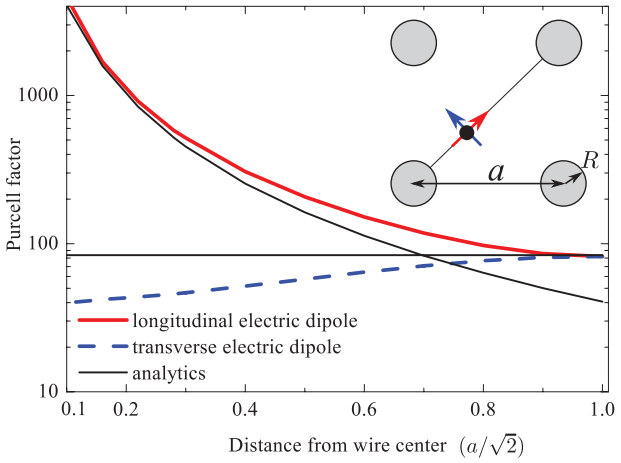

FIG. 5. (Color online) Purcell factor for electric dipole as function of dipole position within the unit cell. Thick solid and dashed curves are results of numerical integration of Eq. (7) for longitudinal and transverse dipole orientation (see geometry scheme in the inset). Thin lines correspond to analytical results Eqs. (34) and (41). Calculation was performed for $\varepsilon_{\text{wire}} \to \infty$, $qa = 0.05\pi$, and $R/a = 0.05$.

general relation between the Purcell factors of electric and magnetic dipoles for perfect wires, holding at any distance from the wires. Equations (41) and (42) constitute the analytical result for in-plane electric and magnetic dipoles positioned close to the wires. For vertical dipoles one has $f_z^{(e)} = 0$ and $f_z^{(m)} = 1$ at $\varepsilon_{\text{wire}} \to \infty$, independent of the dipole coordinates. The general structure of Eq. (41) is the same as for the three-dimensional arrays of resonant dipoles.[24] It consists of two factors; the first factor, proportional to a^2/ρ_0^2, describes the local-field enhancement; the second factor, proportional to $1/(qa)^2$, describes the collective effect—density of states enhancement due to the TEM modes.

A comparison between analytical results Eq. (41) and direct numerical integration of Eq. (7) is presented in Fig. 5. The figure demonstrates the high sensitivity of the Purcell factor to the position and orientation of the dipole. The Purcell factor for the electric dipole, oriented along the radius vector, greatly increases when the dipole approaches the center of the wire. This growth is well described by Eq. (41) (see the thin curve in Fig. 5). In the case of transverse orientation, the Purcell factor is suppressed at small distances from the wire center. The thin horizontal line in Fig. 5 presents the analytical answer Eq. (31) for the Purcell factor of the electric dipole in the lattice center, obtained in Sec. IV A and perfectly agreeing with numerical calculation.

V. APPLICATION TO PARTICULAR STRUCTURES

Next we apply our general theory to realistic experimental structures, operating in microwave[2] and optical[34] frequency ranges. The structure from Ref. 2, used for subwavelength transmission of images, is characterized with the period $a = 1$ cm and wire radius $R = 1$ mm. The asymptotic result Eq. (34) for perfectly conducting wires is valid for microwaves. This result may be explicitly written as

$$f_{x,y}^{(e)} = f_{x,y}^{(m)} = \frac{3\pi c^2}{4\omega^2 a^2} \frac{\ln[1 + \pi/3 + 2\ln(a/2\pi R)]}{\ln(a/2\pi R) + \pi/6}. \quad (43)$$

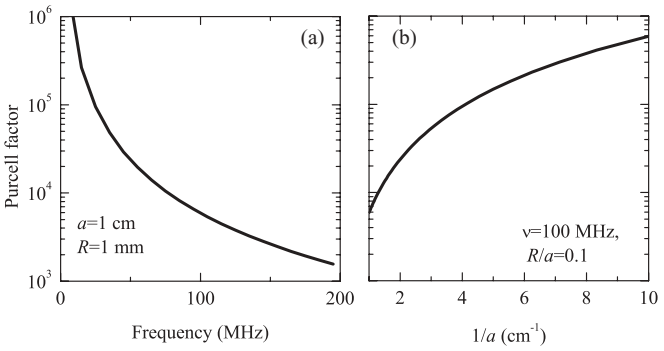

FIG. 6. Purcell factor for wire metamaterial, corresponding to Ref. 29 and operating in microwave frequency range. (a) Frequency dependence for $a = 1$ cm and $R = 0.1a$. (b) Dependence on the lattice constant a for $R = 0.1a$ and $\nu = 0.1$ GHz.

Equation (43) shows that the Purcell factor is directly proportional to the square of the ratio of the wavelength to the lattice constant and only logarithmically depends on the relative thickness of the wires R/a. Dependence of the Purcell factor on the emission frequency ω and the lattice constant is shown in Figs. 6(a) and 6(b), respectively. The Purcell factor strongly increases for smaller frequencies and smaller lattice periods. Calculation demonstrates that the wire medium allows us to achieve high values of the Purcell factor in the whole microwave spectral range.

In the optical frequency range, wire metamaterial may be realized as an array of gold nanowires in alumina.[3,34] The Purcell factor calculated for this structure is presented in Fig. 7. Realistic energy dependence of the dielectric constant of gold nanowires from Ref. 34 has been taken into account. The value $\varepsilon_{\text{out}} = 2.56$ has been used for the dielectric constant of

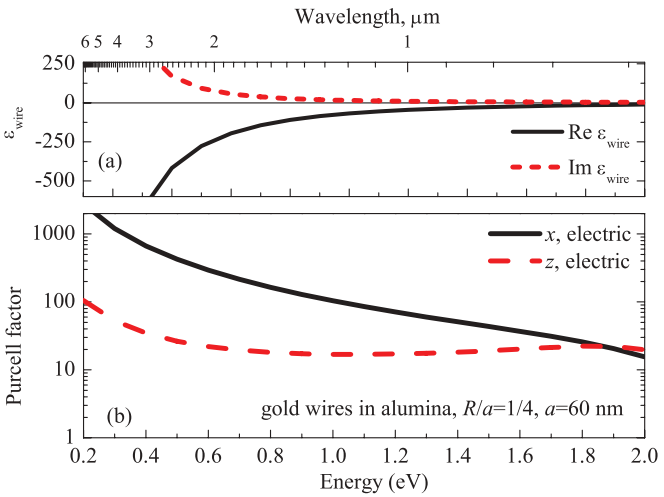

FIG. 7. (Color online) Purcell factor for nanowire metamaterial, corresponding to Ref. 34. (a) Energy dependence of the dielectric constant of the wires. (b) Energy dependence of the Purcell factor for horizontal (black solid curve) and vertical (red dashed curve) electric dipole. Calculation was performed at $a = 60$ nm, $R = a/4$, and $x_0 = y_0 = a/2$. The decay rate is normalized to the value in the bulk matrix.

the alumina matrix. To account for the dielectric constant of the matrix, different from unity, the wire dielectric constant in Eq. (2) was scaled as $\varepsilon_{\text{wire}} \to \varepsilon_{\text{wire}}/\varepsilon_{\text{out}}$, which corresponds to the Purcell factor defined as spontaneous decay enhancement with respect to the bulk matrix. Figure 7 shows that for axial dipole orientation a flat maximum in the Purcell factor with $f \sim 20$ is reached at the energy $E \sim 1.8$ eV. This roughly corresponds to the optimal dielectric constant of the wires, revealed in Fig. 3. For the in-plane dipole the Purcell factor monotonously decays with the photon energy due to the decreasing photonic density of states $\sim 1/(qa)^2$, although its value stays above 10 for all energies below 2 eV. This result also agrees by an order of magnitude with the value $f^{(e)} \sim 6$, experimentally measured in Ref. 7 for dye emission near the nanorod metamaterial. Several issues should be noted regarding the relevance of Fig. 7 to real experimental structure. First, our theory has been derived neglecting the transverse polarization of the wires. This assumption certainly fails at large energies when the light wavelength becomes comparable with the wire thickness. Second, the real nanorods have the lengths in order of hundreds of nm, while in theory they are assumed infinite. Third, the Purcell factor calculated according to Eq. (6) corresponds to the total decay rate caused by electromagnetic interaction with the medium. It is determined by a sum of the rate of photon radiation in the far field and the rate with which the photons are radiated and then reabsorbed due to the dielectric losses.[28] Thus, Eq. (6) overestimates the enhancement of radiation efficiency. Consequently, the curves in Fig. 7 should be considered as an upper boundary of the Purcell factor in the gold nanorod metamaterial, rather than as a modeling for a specific sample of Ref. 34. Still, they indicate that a relatively high Purcell factor may be achieved in the visible spectral range.

VI. CONCLUSIONS

We have developed a general analytical theory of spontaneous emission of both electric and magnetic dipole sources in wire metamaterials. Our theory goes beyond the effective-medium approximation and fully accounts for the discreteness of the structure. We have analyzed the dependence of the Purcell factor on the dipole position within the lattice unit cell as well as on the wire dielectric constant. We have demonstrated that the Purcell factor can be greatly enhanced due to the large density of states of TEM modes, and its value is of the order of a squared ratio of the light wavelength to the lattice constant. The Purcell factor is very sensitive to the position and orientation of the dipole source, and it may increase due to the local-field effect when the dipole approaches the wires. For the electric dipole the spontaneous emission rate grows when the wires are not perfectly conducting. We have found an optimal value of the wire dielectric constant that maximizes the Purcell factor. We have demonstrated the possibility of broadband enhancement of the spontaneous decay rate in realistic wire metamaterials operating in both microwave and optical spectral ranges.

ACKNOWLEDGMENTS

This work was supported by the Ministry of Education and Science of the Russian Federation (Grants No. 11.G34.31.0020,14.B37.21.1649,14.B37.21.1941), the "Dynasty" Foundation, the Russian Foundation for Basic Research (Grants No. 12-02-12097,12-02-00757,12-02-33034), European Union (projects POLAPHEN and SPANLG4Q), and the Australian Research Council. The authors acknowledge useful discussions with C. R. Simovski and A. E. Miroshnichenko.

*a.poddubny@phoi.ifmo.ru

[1] C. R. Simovski, P. A. Belov, A. V. Atrashchenko, and Y. S. Kivshar, Adv. Mater. **24**, 4229 (2012).
[2] P. A. Belov, Y. Zhao, S. Tse, P. Ikonen, M. G. Silveirinha, C. R. Simovski, S. Tretyakov, Y. Hao, and C. Parini, Phys. Rev. B **77**, 193108 (2008).
[3] G. A. Wurtz, W. Dickson, D. O'Connor, R. Atkinson, W. Hendren, P. Evans, R. Pollard, and A. V. Zayats, Opt. Express **16**, 7460 (2008).
[4] R. J. Pollard, A. Murphy, W. R. Hendren, P. R. Evans, R. Atkinson, G. A. Wurtz, A. V. Zayats, and V. A. Podolskiy, Phys. Rev. Lett. **102**, 127405 (2009).
[5] A. V. Kabashin, P. Evans, S. Pastkovsky, W. Hendren, G. A. Wurtz, R. Atkinson, R. Pollard, V. A. Podolskiy, and A. V. Zayats, Nat. Mater. **8**, 867 (2009).
[6] M. A. Noginov, Y. A. Barnakov, G. Zhu, T. Tumkur, H. Li, and E. E. Narimanov, Appl. Phys. Lett. **94**, 151105 (2009).
[7] M. A. Noginov, H. Li, Y. A. Barnakov, D. Dryden, G. Nataraj, G. Zhu, C. E. Bonner, M. Mayy, Z. Jacob, and E. E. Narimanov, Opt. Lett. **35**, 1863 (2010).
[8] J. Yao, Z. Liu, Y. Liu, Y. Wang, C. Sun, G. Bartal, A. M. Stacy, and X. Zhang, Science **321**, 930 (2008).
[9] F. Lemoult, M. Fink, and G. Lerosey, Nat. Commun. **3**, 889 (2012).
[10] V. V. Vorobev and A. V. Tyukhtin, Phys. Rev. Lett. **108**, 184801 (2012).
[11] D. E. Fernandes, S. I. Maslovski, and M. G. Silveirinha, Phys. Rev. B **85**, 155107 (2012).
[12] M. G. Silveirinha and S. I. Maslovski, Phys. Rev. B **85**, 155125 (2012).
[13] P. A. Belov, R. Marqués, S. I. Maslovski, I. S. Nefedov, M. Silveirinha, C. R. Simovski, and S. A. Tretyakov, Phys. Rev. B **67**, 113103 (2003).
[14] M. G. Silveirinha, Phys. Rev. E **73**, 046612 (2006).
[15] Z. Jacob and V. M. Shalaev, Science **334**, 463 (2011).
[16] H. N. S. Krishnamoorthy, Z. Jacob, E. Narimanov, I. Kretzschmar, and V. M. Menon, Science **336**, 205 (2012).
[17] A. N. Poddubny, P. A. Belov, and Y. S. Kivshar, Phys. Rev. A **84**, 023807 (2011).
[18] O. Kidwai, S. V. Zhukovsky, and J. E. Sipe, Opt. Lett. **36**, 2530 (2011).
[19] C. V. Vlack and S. Hughes, Opt. Lett. **37**, 2880 (2012).
[20] H. T. Dung, L. Knöll, and D.-G. Welsch, Phys. Rev. A **65**, 043813 (2002).
[21] W. Yan, M. Wubs, and N. A. Mortensen, Phys. Rev. B **86**, 205429 (2012).

[22]I. Iorsh, A. Poddubny, A. Orlov, P. Belov, and Y. S. Kivshar, Phys. Lett. A **376**, 185 (2012).
[23]O. Kidwai, S. V. Zhukovsky, and J. E. Sipe, Phys. Rev. A **85**, 053842 (2012).
[24]A. N. Poddubny, P. A. Belov, P. Ginzburg, A. V. Zayats, and Y. S. Kivshar, Phys. Rev. B **86**, 035148 (2012).
[25]C. L. Cortes, W. Newman, S. Molesky, and Z. Jacob, J. Opt. **14**, 063001 (2012).
[26]S. I. Maslovski and M. G. Silveirinha, Phys. Rev. A **83**, 022508 (2011).
[27]E. M. Purcell, Phys. Rev. **69**, 681 (1946).
[28]M. Glazov, E. Ivchenko, A. Poddubny, and G. Khitrova, Phys. Solid State **53**, 1753 (2011).
[29]P. Belov, S. Tretyakov, and A. Viitanen, JEWA **16**, 1153 (2002).
[30]E. L. Ivchenko, *Optical Spectroscopy of Semiconductor Nanostructures* (Alpha Science International, Harrow, 2005).
[31]L. Novotny and B. Hecht, *Principles of Nano-Optics* (Cambridge University Press, New York, 2006).
[32]X. Wang, X.-G. Zhang, Q. Yu, and B. N. Harmon, Phys. Rev. B **47**, 4161 (1993).
[33]R. E. Collin, *Field Theory of Guided Waves* (McGraw-Hill, New York, 1960).
[34]R. Atkinson, W. R. Hendren, G. A. Wurtz, W. Dickson, A. V. Zayats, P. Evans, and R. J. Pollard, Phys. Rev. B **73**, 235402 (2006).